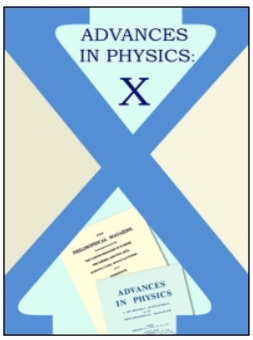

Advances in Physics: X

ISSN: (Print) 2374-6149 (Online) Journal homepage: http://www.tandfonline.com/loi/tapx20

Recent breakthroughs in scanning transmission electron microscopy of small species

Karel Hendrik Wouter van den Bos, Thomas Altantzis, Annick De Backer, Sandra Van Aert & Sara Bals

To cite this article: Karel Hendrik Wouter van den Bos, Thomas Altantzis, Annick De Backer, Sandra Van Aert & Sara Bals (2018) Recent breakthroughs in scanning transmission electron microscopy of small species, Advances in Physics: X, 3:1, 814-832, DOI: 10.1080/23746149.2018.1480420

To link to this article: https://doi.org/10.1080/23746149.2018.1480420

© 2018 The Author(s). Published by Informa UK Limited, trading as Taylor & Francis Group.

Published online: 13 Aug 2018.

Submit your article to this journal

Article views: 43

View Crossmark data

Full Terms & Conditions of access and use can be found at
http://www.tandfonline.com/action/journalInformation?journalCode=tapx20

ADVANCES IN PHYSICS: X
2018, VOL. 3, NO. 1, 814–832
https://doi.org/10.1080/23746149.2018.1480420

Taylor & Francis
Taylor & Francis Group

OPEN ACCESS Check for updates

Recent breakthroughs in scanning transmission electron microscopy of small species

Karel Hendrik Wouter van den Bos, Thomas Altantzis, Annick De Backer, Sandra Van Aert and Sara Bals

EMAT, University of Antwerp, Antwerp, Belgium

ABSTRACT

Over the last decade, scanning transmission electron microscopy has become one of the most powerful tools to characterise nanomaterials at the atomic scale. Often, the ultimate goal is to retrieve the three-dimensional structure, which is very challenging since small species are typically sensitive to electron irradiation. Nevertheless, measuring individual atomic positions is crucial to understand the relation between the structure and physicochemical properties of these (nano)materials. In this review, we highlight the latest approaches that are available to reveal the 3D atomic structure of small species. Finally, we will provide an outlook and will describe future challenges where the limits of electron microscopy will be pushed even further.

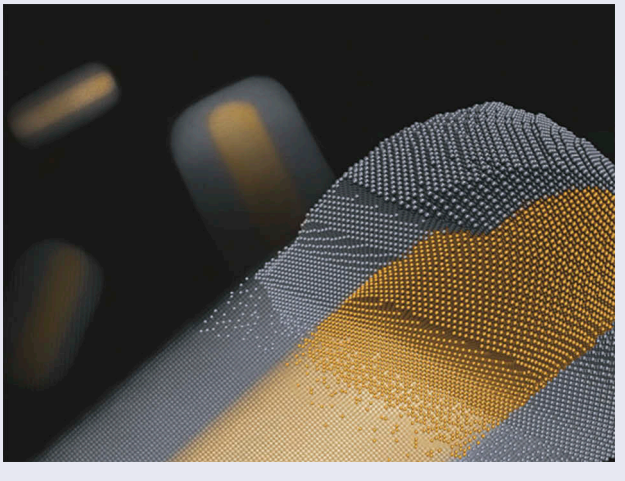

Abbreviations: 2D: Two-dimensional; 3D: Three-dimensional; FAU: Faujasite; GPU: graphical processing unit; HAADF: High angle annular dark field; ICL: Integrated classification likelihood; SNR: Signal-to-noise ratio; STEM: Scanning transmission electron microscopy; XRD: X-ray diffraction

ARTICLE HISTORY
Received 30 March 2018
Accepted 21 May 2018

KEYWORDS
STEM imaging; atom-counting; statistical parameter estimation theory; nanomaterials; beam-sensitive; 3D atomic structure

PACS
31.15.bt; 61.05.jd; 61.46.Df; 68.37.Ma

CONTACT Sara Bals Sara.Bals@uantwerpen.be

© 2018 The Author(s). Published by Informa UK Limited, trading as Taylor & Francis Group.
This is an Open Access article distributed under the terms of the Creative Commons Attribution License (http://creativecommons.org/licenses/by/4.0/), which permits unrestricted use, distribution, and reproduction in any medium, provided the original work is properly cited.

Introduction

In this age of nanotechnology, there is a constant demand to develop novel and innovative nanostructures with predefined properties. Reducing the size of materials to the nanometre level not only allows the design of more compact devices, but also can be used as a route towards the enhancement of the material properties or may even enable the design of novel functionalities [1,2]. Essentially, nanomaterials can be considered as a three-dimensional (3D) agglomeration of atoms. Therefore, their properties are determined by the positions of the atoms, their chemical nature and the bonding between them. If one is able to determine these parameters in 3D, it becomes possible to provide the necessary input to predict the physicochemical properties. The rational design of nanomaterials with optimised functional properties therefore strongly depends on the availability of advanced quantitative 3D characterisation techniques. In this manner, materials science can evolve towards a system where new materials with specific properties can be designed before actual production [3–5].

Aberration-corrected scanning transmission electron microscopy (STEM) is an excellent tool to characterise nanostructures as it provides two-dimensional (2D) projected images that are sensitive to the local 3D structure of the studied sample [6–9]. When studying nanostructures, STEM has major advantages in comparison to X-ray diffraction (XRD) since it enables one to investigate deviations from perfect crystallinity [10,11]. The schematics of STEM imaging are represented in Figure 1. A focussed electron probe is created by the condenser lens system and is scanned according to a two-dimensional (2D) raster over the object. The total amount of electrons scattered towards an annular detector is integrated and displayed as a function of probe position. The resulting image contrast depends largely on the collection range of the detector [12,13]. Often, high angle annular dark field (HAADF) STEM is used, where the inner collection angle of the detector β_1 is much larger than the probe convergence semi-angle α. In this setup, mainly Rutherford scattered electrons are recorded, which vary approximately as Z^2 [14,15]. As a consequence, the image contrast in HAADF STEM imaging is incoherent and depends largely on the crystal thickness and the atomic number Z. Therefore, these images are suitable for a quantitative interpretation.

Over the years, the improved quality and stability of the electromagnetic lenses together with the development of aberration correctors have greatly improved the resolution of the STEM images. Nowadays, nanostructures can be visualised with a resolution of the order of 50 pm [8,16–18], which is approximately equal to the size of the electrostatic potential of most atoms. Often, atomically resolved HAADF STEM images are considered as a final result and the structure is interpreted visually from such images. Here, we will show

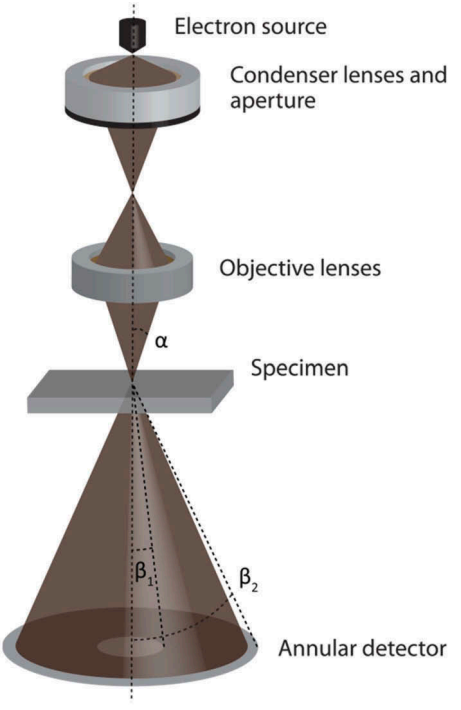

Figure 1. Schematic drawing of a STEM instrument. A focussed electron beam with convergence semi-angle α is raster-scanned over the specimen. Scattered electrons are collected by an annular detector with inner and outer angle β_1 and β_2, respectively.

that a quantitative analysis of the experimental data is vital for a correct representation of the results.

In practice, experimental images are subjected to image distortions or a low signal-to-noise ratio (SNR), which hampers any analysis. Therefore, advanced post-processing techniques that enhance the SNR of the images are of great importance [19–23]. However, structural information should also be extracted on a local scale. For this purpose, statistical parameter estimation theory has been proven to be an excellent tool as it can quantitatively measure structure parameters, such as, the 2D atomic column positions, number of atoms along the viewing direction, or composition, with the highest attainable precision [24–26].

It is, however, still not straightforward to obtain the 3D atomic positions of nanostructures. Indeed, one may never forget that all images acquired by electron microscopy are only 2D images of a 3D object. Electron tomography has therefore been developed as a powerful tool to investigate the morphology, 3D structure and composition of a broad range of materials [27,28]. Many results have been achieved at the nanometre level, but different open questions in materials science demanded the

further development of the technique and have pushed the resolution to the atomic level.

Most high-resolution studies in 3D have been carried out for relatively stable materials. Unfortunately, for small species, it is far from straightforward to acquire a large number of TEM images. One of the main reasons is related to the sensitivity of such samples under electron irradiation, which may cause structural changes during imaging. To minimise the energy transfer from the incident electron beam to the sample, a lower acceleration voltage and acquisition time may be used if one retains sufficient image resolution, contrast, and pixel SNR. Hereby, advanced methods such as statistical parameter estimation are again required to retrieve 3D structural information that can be used to understand the structure–properties relationship.

In this review article, an overview of quantitative methods which are often applied to characterise small species in the field of STEM will be given. We will show that unknown structure parameters, including atomic positions, the number of atoms and chemical concentrations, can be determined with picometre range precision from experimental images. Furthermore, it will be demonstrated how the combination of state-of-the-art electron microscopy and advanced computational methods enables the investigation of the 3D atomic structure of nanoparticles and small clusters.

2. From qualitative to quantitative electron microscopy

Aberration-corrected HAADF STEM imaging provides atomically resolved incoherent images that can be used for a visual 2D structural and chemical characterisation. In addition, these images may serve as an input for quantitative interpretation methods. Over the last decade, advanced image processing techniques have become available that can enhance the SNR of the experimental images [19–23] or that can be used to determine atomic column positions and image intensities precisely [24–26]. For small species, these methods will be described below.

2.1 *Improving the signal-to-noise ratio by template matching*

Very often, nanostructures are sensitive to electron irradiation and the observation time by electron microscopy is usually limited to a few seconds, making their characterisation very challenging. In order to reduce the effect of the beam, and minimise any structural changes, it is of great importance to keep the electron dose to a strict minimum. Unfortunately, this results in a low SNR in the obtained images. To overcome this problem, a template matching procedure can be applied to the acquired data. This technique enables one to find specific regions in a given image that correspond to a pre-defined template [29]. By averaging these regions, the SNR will

significantly increase in comparison to the raw data, enabling structural investigations. As an example, the characterisation of oligo-atomic Ag clusters confined in faujasite (FAU) zeolites will be discussed [30].

Thermal treatment of Ag-exchanged zeolites yields highly luminescent Ag clusters, where the cluster configuration determines the emission colour [31]. Therefore, a non-activated and a heat-activated sample have been investigated. HAADF STEM images of both samples are shown in Figure 2(a,b) and Figure 2 (e,f). Since these materials are extremely sensitive to electron irradiation [32–34], a low incident electron dose was used. In order to improve the SNR, the template matching procedure was applied resulting in averaged images displayed in Figure 2(c,d) and 2(g,h). Due to the Z-contrast in HAADF STEM images, it can be assumed that the bright spots in the averaged images correspond to the projected positions of the Ag atoms in the zeolitic framework (Si, Al and O). However, from these images it is clear that the intensities of the bright spots are

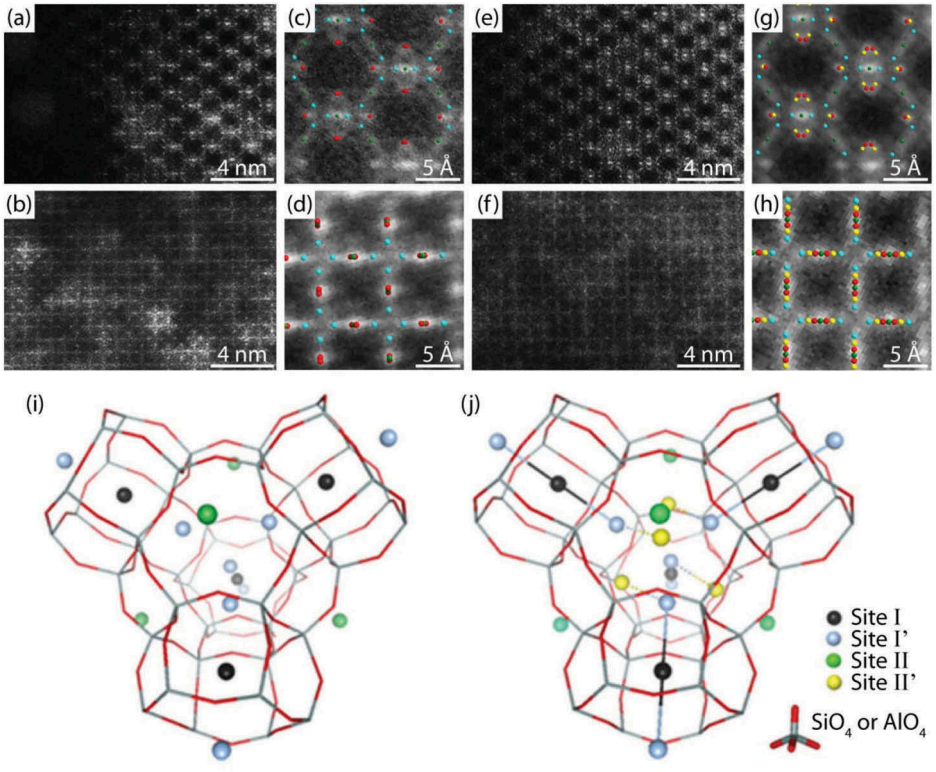

Figure 2. HAADF STEM images of Ag-FAUX zeolites in (a) [110] and (b) [100] zone-axis orientation for the cation-exchanged sample and (e) [110] and (f) [100] zone-axis orientation for the heat-treated sample (c,d,g,h). Averaged images obtained by template matching for (a), (b), (e) and (f), respectively. The silver atomic positions are shown as an overlay, where the colours represent Ag atoms with different occupancy factors. The 3D structural models for the Ag-FAUX zeolites in their (i) non-luminescent and (j) luminescent states. Adapted with permission from Altantzis *et. al* [30]. Copyright 2016 American Chemical Society.

not equal, which is explained by the presence of multiple Ag atoms along the same projected position. By combining these results to complementary XRD, 3D structural models of the Ag clusters could be proposed for the non-luminescent and luminescent states, which are displayed in Figure 2(i,j). As can be seen in Figure 2(j), interatomic distances slightly decrease and a migration of Ag atoms from site II to site II' takes place in the heat-activated form. Based on these Ag positions, it is concluded that a tetranuclear $[Ag_3 \cdots Ag]$ silver species is formed, which is most likely responsible for the light absorption and emission.

2.2. *Statistical parameter estimation theory: measuring atomic positions with picometre precision*

Although template matching could improve the SNR in an image, the resulting analysis still only provides averaged information. Therefore, alternative approaches are required to investigate nanostructures and small clusters on a more local scale. Ideally, atomic positions should be measured with picometre precision as materials properties do already alter when atoms are displaced in this range. For this purpose, statistical parameter estimation theory has been introduced [35,36]. This theory relies on the availability of a parametric model to describe the expectations of the experimental image. The combination of this technique with HAADF STEM images has the potential to determine structure parameters, such as atomic column positions, with a precision that can far exceed the resolution of the microscope [37,38]. Therefore, it enables one to identify structural changes, even when a visual interpretation is no longer possible [24]. For atomic resolution HAAFDF STEM images of crystalline structures, acquired along a major zone-axis, image intensities peak at the atomic column positions and can be modelled as a superposition of Gaussian functions [39,40]. The unknown parameters are estimated by fitting this model to the experimental images using a criterion of goodness of fit quantifying the similarities between the experimental images and the model. Recently, a new user-friendly program, called StatSTEM, has been released, which contains an efficient implementation of this model-based quantification methodology, allowing one to accurately extract structure parameters from atomically resolved STEM images with the highest attainable precision [25].

The potential and applicability of the approach is presented in the following example in which we investigated the effect of atomic dopants on the lattice parameters and the properties of $CsPbBr_3$ nanocrystals [41]. By exchanging Pb^{2+} atoms with Sn^{2+}, Cd^{2+} or Zn^{2+} cations in colloidal $CsPbBr_3$ nanocrystals, a blue-shift in the optical spectra has been observed. To understand this effect, HAADF STEM images, acquired using a probe aberration-corrected FEI Titan^3 operated at 300 kV, have been quantified using statistical parameter estimation theory (see Figure 3). From the measured Pb/halide column positions, the lattice parameters of the undoped and doped crystals are

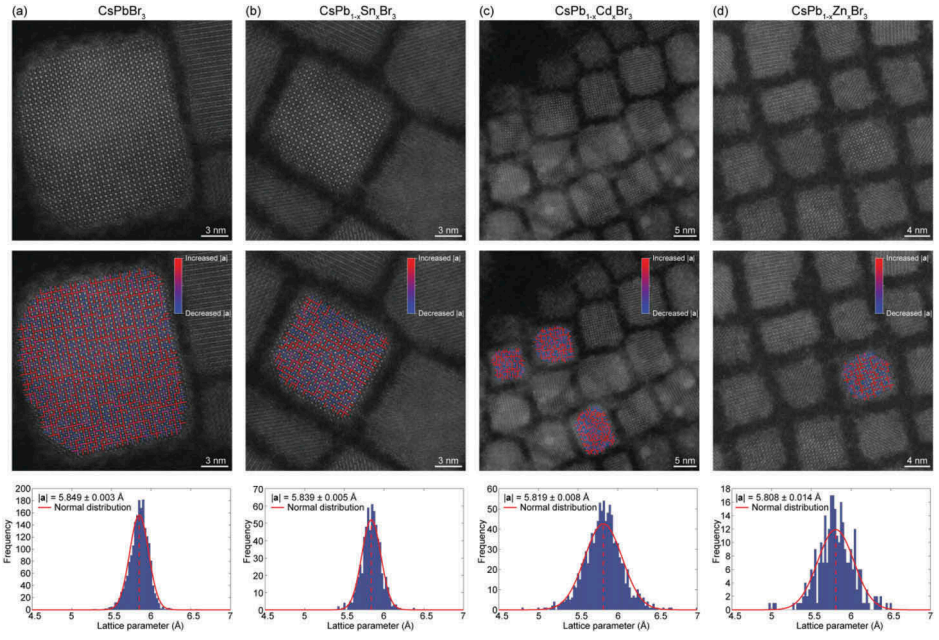

Figure 3. Lattice parameter measurements on HAADF STEM images of (a) undoped and (b) Sn-,(c) Cd-, and (d) Zn-doped $CsPbBr_3$ nanocrystals. Blue and red bars indicate smaller and larger lattice spacings than the mean value in undoped $CsPbBr_3$ nanocrystals, $|a| = 5.85$ Å. The histograms of lattice parameters reveal a lattice contraction of the doped $CsPbBr_3$ nanocrystals. Reprinted with permission from van der Stam *et. al* [41]. Copyright 2017 American Chemical Society.

calculated. By fitting a normal distribution to these distance estimates, the mean lattice parameter has been determined. The lattice parameter of the parent $CsPbBr_3$ nanocrystals has been calibrated to the value reported in literature for the cubic perovskite structure of $CsPbBr_3$ [42]. A lattice contraction from $|a| = 5.849 \pm 0.003$ Å to $|a| = 5.839 \pm 0.005$ Å is observed when exchanging Pb^{2+} atoms with Sn^{2+}. Similar analyses on $CsPbBr_3$ nanocrystals doped with Cd^{2+} and Zn^{2+} shows a lattice contraction from $|a| = 5.849 \pm 0.003$ Å to $|a| = 5.819 \pm 0.008$ Å and $|a| = 5.808 \pm 0.014$ Å, respectively. The lattice contraction for the Cd- and Zn-dopants (0.5 and 0.7%, respectively) is larger than that for the Sn-dopants, which is in full agreement with electron diffraction measurements [38]. This difference is expected based on the ionic radii of the divalent cations, which is for Pb^{2+} 119 pm, Sn^{2+} 118 pm, Cd^{2+} 95 pm, and Zn^{2+} 74 pm [43]. Since no clusters with small or large lattice vectors are observed in Figure 3, the results suggest that the dopants are homogeneously distributed throughout the nanocrystals. These observations demonstrate the importance to measure local structure parameters precisely.

3. Atomic resolution electron tomography of nanoparticles

As described in the previous section, quantitative methods enable the investigation of nanostructures at the atomic scale. HAADF STEM images are, however, 2D projections of 3D objects. Electron tomography can be used to overcome this limitation. Here, images of the object are acquired at different tilt angles [28,44]. Then, after carefully aligning the recorded images with respect to each other and along a common axis [45,46], a 3D reconstruction of the object can be obtained by using them as an input for a mathematical algorithm. In addition to the morphology, the crystal structure, including defects and (surface) strain, is equally essential, since it will directly affect the properties [47,48]. Being able to perform electron tomography with atomic resolution is therefore crucial. Especially for small species, 3D studies are only of interest when performed at the atomic scale, given the size of the clusters. Although this is not yet a standard possibility for all structures, significant progress has recently been achieved using different approaches.

3.1 *Three dimensional atomic resolution of model like structures*

The first visualisations of the 3D atomic structure of a nanoparticle were based on a single 2D projection image. The projected intensities of atomically resolved HAADF STEM images acquired from an isolated Au nanocluster were quantitatively analysed. In this manner, Li et al. were able to extract a thickness profile and to propose a 3D model [49]. In 2011, our group performed a 3D reconstruction at the atomic scale for a 3 nm Ag nanoparticle embedded in an Al matrix [50]. The reconstruction was based on two HAADF STEM images acquired along different zone axes. Using statistical parameter estimation theory, the number of atoms in each atomic column was determined. A particularly useful performance measure for atom-counting is the so-called scattering cross-section, which is defined as the total intensity of scattered electrons by a single atomic column [24,51]. This quantity can be measured either by integrating the image contributions of an atomic column [51] or by estimating the volume under a Gaussian peak describing the shape of the image of an atomic column [26,50,52,53]. The scattering cross-section is robust to microscope parameters such as magnification, defocus, astigmatism and source size broadening [51,54,55]. Since it increases monotonically with thickness, it is extremely suitable to count the number of atoms in each atomic column [56]. A second advantage of the scattering cross-sections in HAADF STEM imaging is that they are also sensitive to the composition.

In Figure 4, aberration-corrected HAADF STEM images of the Ag cluster are modelled as a superposition of Gaussian peaks using statistical parameter estimation theory. From the estimated parameters, scattering cross-sections have been calculated for each column, which are shown for the $[10\bar{1}]$ zone-axis orientation in the histogram in Figure 4(d). It is expected that the thickness of the substrate is constant over the particle, leading to an increase in intensity when substituting an Al atom by an Ag atom. The presence of noise smears out the peaks, making a visual interpretation in terms of the number of atoms often impossible or highly subjective. Therefore, the scattering cross-sections in the histogram are regarded as independent statistical draws from a Gaussian mixture model. By evaluating the so-called integrated classification likelihood (ICL) criterion, shown in Figure 4(e), ten significant peaks in the histogram are identified as a local minimum. Finally, the locations of the peaks in the selected Gaussian mixture model are used to assign the number of Ag atoms for each atomic column, leading to the results shown in Figure 4(c). In a similar manner, counting results are obtained for the [100] direction, as shown in Figure 4(f)–4(h). Afterwards, discrete tomography was used to combine the counting results into a 3D reconstruction with atomic resolution (see Figure 4(i)) [51]. The discreteness that is exploited here is the fact that crystals can be thought of as discrete assemblies of atoms. An excellent match was found when comparing the 3D reconstruction with additional projection images that were acquired along different zone axes. The same method has been used to reconstruct the core of a free-standing PbSe-CdSe core-shell nanorod [57].

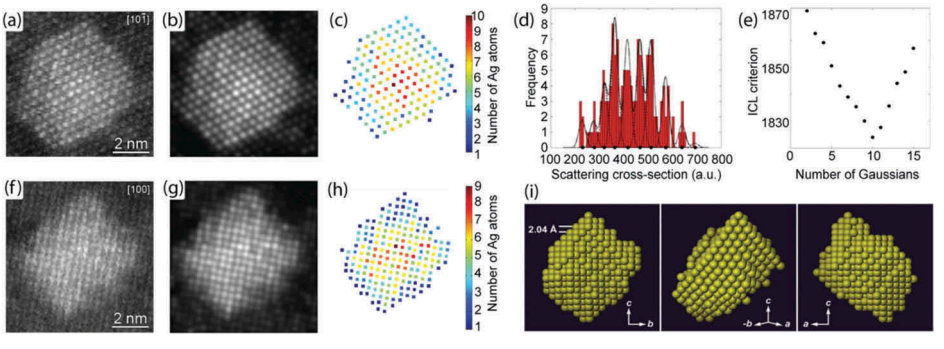

Figure 4. HAADF STEM images of nanosized Ag clusters embedded in an Al matrix in (a) $[10\bar{1}]$ and (f) [100] zone-axis orientation. (b,g) Refined parameterised models of the images (a) and (b) (c,h). The number of Ag atoms per column. (d) Histogram of scattering cross-sections of the Ag columns in (b). (e) Integrated classification likelihood (ICL) criterion evaluated as a function of the number of Gaussians in the mixture model describing the histogram (d). (i) The computed 3D reconstruction of the Ag nanocluster. Adapted by permission from Macmillan Publishers Limited, Nature, Three-dimensional atomic imaging of crystalline nanoparticles, Van Aert *et. al* [50]., copyright 2011.

After these initial studies, different methodologies were proposed to obtain 3D reconstructions using a limited number of projection images [58,59] or using continuous tilt series [46,60]. In this manner, the position of the atoms could be accurately determined in 3D and also 3D strain measurements became possible [61,62]. Recently, also disordered structures could be unraveled and linked to the 3D properties of the nanomaterial [63]. Our group was even able to characterize a disordered structure including vacancies and to determine the effect on the optical properties [64].

3.2 *Three dimensional atomic resolution of heterogeneous nanostructures*

The incorporation of more than one element in the same nano-object has been recently selected as a route towards the synthesis of nanostructures with enhanced properties such as stability, catalytic activity and electrical response [65,66]. However, atom-counting applications on hetero-nanostructures are significantly more complex since HAADF STEM image intensities depend both on thickness and composition. Often a linear dependence on concentration is assumed in compositional studies, although small changes in the atom ordering in the column can modify the scattering cross-sections [24,56,67,68]. Therefore, a quantitative method is required that is capable of recognising all possible 3D column configurations. For example, already more than 2×10^6 column configurations exist for a 20-atom-thick binary alloy having all possible ratios between both elements. Image simulations can provide this information, but the amount of required simulations makes it an impossible task in terms of computing time. In order to overcome these limitations, the atomic lensing model has been developed that can predict the scattering cross-sections in HAADF STEM images [68]. In this model, each atom is described as a lens focussing the incident electrons on the next atom. Lensing factors of the individual atoms can be calculated from image simulations of monotype atomic columns to predict the scattering cross-sections of mixed columns. This approach leads to an accurate prediction of scattering cross-sections which is not restricted to the number of atom types. In this manner, the atomic lensing model facilitates the extension of the atom-counting methodology from homogeneous to heterogeneous nanostructures.

The ability to unravel the 3D composition at the atomic scale is demonstrated in Figure 5, where an experimental HAADF STEM image of an Au@Ag core-shell nanorod has been investigated. Counting results on the pure Ag shell region have been used to estimate the thickness of the nanorod, which limited the number of variables that needs to be predicted. Here, counting results are put on an absolute scale by combining both the simulation- and statistics-based atom-counting method. The atomic lensing model indicated that the dependency of the scattering cross-sections on the atom ordering is less

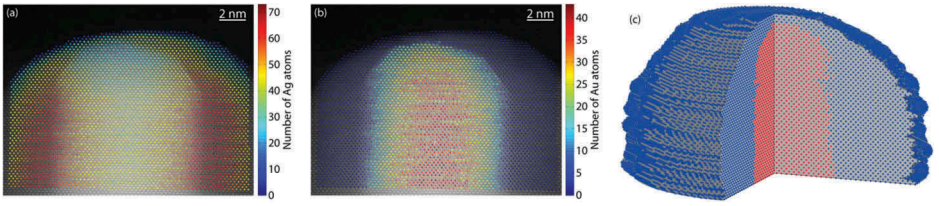

Figure 5. (a,b) Number of Ag and Au atoms counted from an experimental HAADF STEM image of a Ag-coated Au nanorod. (c) The reconstructed 3D atomic model of the nanorod. Reprinted with permission from van den Bos *et. al*., Physical Review Letters, 116, 246,101, 2016 [68]. Copyright 2016 by the American Physical Society.

pronounced in the thickness range of the nanorod. Therefore, the number of Au and Ag atoms could be determined by a direct comparison between measured scattering cross-sections and predicted values, shown in Figure. 5(a) and 5(b). By using a combination of counting results obtained from an additional viewing direction with prior knowledge concerning the shape of the nanorod, a 3D atomic model could be reconstructed, presented in Figure 5(c).

3.3 *Three dimensional* characterisation *of beam sensitive and dynamic structures with atomic resolution*

In the previous examples, images acquired along different zone-axes are required to retrieve the 3D atomic structure. As mentioned before, small species are extremely sensitive to electron irradiation and damage often occurs, even after the acquisition of a single image. For these materials, an alternative approach to retrieve the 3D atomic structure is to use atom-counting results from a single viewing direction as an input in an energy minimisation algorithm using molecular dynamics [69]. In this approach, a starting 3D configuration is obtained by positioning the atoms on a perfect crystal grid symmetrically arranged around a central plane. Then, the potential energy of the 3D configuration is minimised in a Monte Carlo-based approach, where in each iteration step one atomic column is shifted over one unit cell. The new configuration is only kept if the total energy decreases, which is calculated by using a Lennard-Jones potential. The final 3D atomic structure is obtained when convergence is reached. To illustrate the power of this method, beam-sensitive PbSe nanocrystals will be discussed [70].

By using oriented attachment of PbSe nanocubes, 2D superstructures can be formed with long-range nanoscale and atomic order [70]. This superimposed geometry can result in Dirac-type valence and conduction bands and high charge carrier mobility in semiconductors [71,72]. An HAADF STEM image has been recorded to study the degree of coherency inside the superlattice, shown in Figure 6(a). Next, atom-counting results obtained by the statistics-

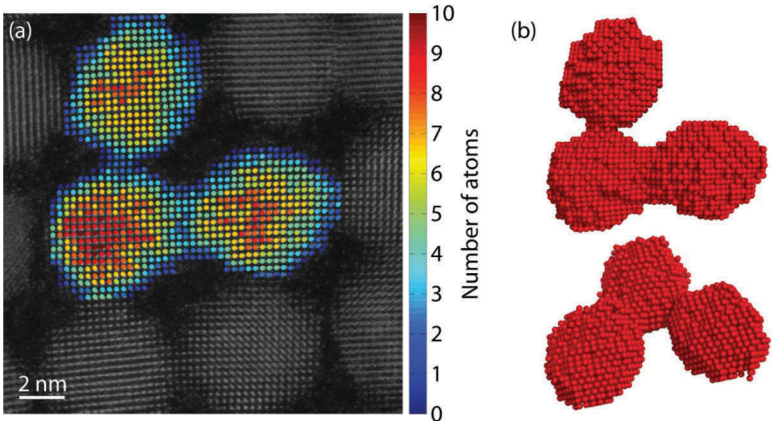

Figure 6. (a) HAADF STEM image with atom-counting results on PbSe nanocrystals following a 2D coherent superstructure. (b) Top and side view of the reconstructed 3D atomic model of the structure shown in (a). Adapted by permission from Macmillan Publishers Limited, Nature Materials, *In situ* study of the formation mechanism of two-dimensional superlattices from PbSe nanocrystals, Geuchies *et. al* [70]., Copyright 2016.

based method have been used as an input to retrieve the 3D atomic structure of these nanocrystals, visualised in Figure 6(b). From this result, it was concluded that there is atomic coherence and that the interface is formed via a so-called necking process [70]. In a similar manner, it was found that the shape of these PbSe nanocrystals is controlled by the ligand density [73].

Since this new approach uses only images acquires along a single viewing direction, it opens up the possibility to study the dynamics of small species. As an illustration, the surface facets of an Au nanodumbbell on an *in situ* heating holder have been characterised [74]. In Figure 7, HAADF STEM images indicate that after heating up to 330°C the nanodumbbell underwent a morphological transition to a nanorod. In the 3D reconstructions, clear surface facets are observed for the entire tip of the nanodumbbell and nanorod. Furthermore, a growth of low index surface facets is seen when heating the nanodumbbell, which can alter the catalytic activity of the particle. As the reconstructions of this method are in excellent agreement with electron tomography [74], it provides a powerful tool to study the physical behaviour of nanomaterials.

4. Small, smaller, smallest

Recent advances in the field of nanotechnology enable the development of smaller and more complex nanostructures, which in turn forces us to push the limits of electron microscopy even further. Ultra-small sub-nanometre nanoparticles or clusters are a typical example of such challenging nanomaterials. Although there is a clear need for a complete characterisation of such materials

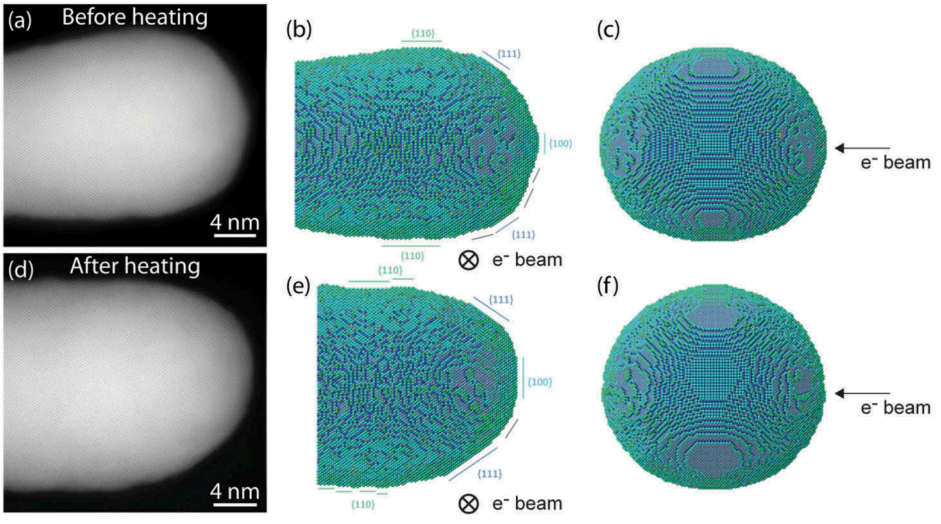

Figure 7. (a,d) HAADF STEM images of Au dumbbell/rod before and after heating. Reconstructed 3D atomic models along different viewing direction for (b,c) the Au dumbbell before heating and (e,f) the Au rod after heating. Adapted from De Backer *et. al* [74]. with permission of The Royal Society of Chemistry.

in 3D, as they can no longer be considered as periodic objects, this is far from straightforward. Rotations of the clusters, as well as structural changes that may occur during investigations by STEM are the main bottlenecks hampering a complete 3D characterisation [49]. Therefore, electron tomography methods that combine different projected images can no longer be applied. Furthermore, the aperiodicity frustrates investigations assuming atoms to be located on a crystal lattice. However, these dynamic changes provide a unique opportunity to investigate the transformations between energetically excited configurations of a cluster, as was noticed by our group when studying an ultra-small Ge cluster consisting of less than 25 atoms [75]. In their study, a series of 2D aberration-corrected HAADF STEM images were collected and analysed using statistical parameter estimation theory. In this manner, the number of atoms was determined at each position, as illustrated in Figure 8. As no prior knowledge of the structure was available, *ab initio* calculations were carried out to extend these 2D counting results to 3D structural models. In this procedure, several starting configurations were constructed from the 2D atomic positions and counting results. Only the configurations in which a planar base structure was assumed were still consistent after full relaxation with the experimental HAADF STEM images. As visualised in Figure 8, all relaxed cluster configurations stay relatively close to their starting structures. Therefore, reliable 3D models can be obtained by combining counting results with *ab initio* calculations. Furthermore, by tracking the path of each individual atom the dynamics of the cluster can be investigated.

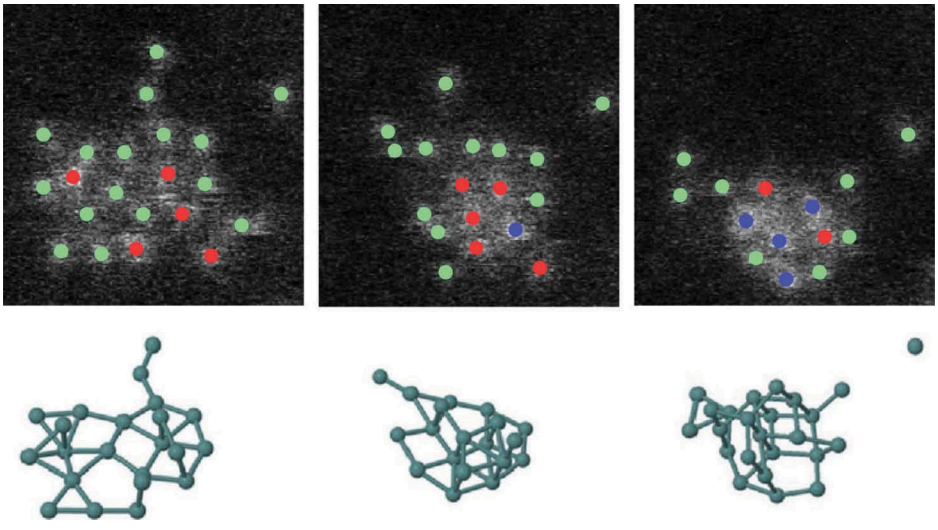

Figure 8. HAADF STEM images with counting results for three different configurations of an ultra-small Ge cluster (top row). Green, red, and blue dots correspond to one, two, and three atoms, respectively. The 3D model obtained by *ab initio* calculations are shown below. Adapted by permission from Macmillan Publishers Limited, Nature Communications, Atomic scale dynamics of ultrasmall germanium clusters, Bals *et. al* [75]., copyright 2012.

5. Conclusions and outlook

Over the past years, major advances have been made in the field of scanning transmission electron microscopy to investigate the 3D atomic structure of small species. Here, the main challenge is to minimise the electron irradiation while maintaining sufficient resolution and image quality. For this purpose, different methods have been discussed that can retrieve 3D structural information from only a limited number of HAADF STEM images. Here, it has been demonstrated that statistical parameter estimation theory is a useful tool to measure unknown structure parameters with high precision, including atomic positions and types. These results act as an input for reconstruction algorithms that can retrieve the 3D atomic structure. In order to minimise structural changes, electron irradiation should be kept as low as possible. For these materials, methods have been presented that can retrieve 3D structural information by combining counting results from two different images. Furthermore, when combining counting results from only a single image with an energy minimisation algorithm or *ab initio* calculations, the 3D structure can be revealed. These last approaches even allow one to study the dynamics of particles by analysing time-series of images [69,74,75].

The ultimate goal of aberration-corrected HAADF STEM imaging of small clusters is to measure their 3D atomic structure and composition with picometre precision. For this purpose, the principles of statistical experiment design enable one to optimise the microscope and detector settings and explore the

fundamental limits given by the microscope itself [76–81]. This is especially important as new detector geometries have been proposed which can, for example, collect scattered electrons in different annular regimes or on a pixel array grid [82–90]. The simultaneous acquisition of different detector regimes can reveal both light and heavy elements and is, therefore, a powerful method to study the 3D atomic structure of heterogeneous nanomaterials. These developments will certainly open up new possibilities to characterise and understand the structure-property relation of small species, but working with these detectors is computationally demanding by the large amount of data that needs to be processed. The future development of smart algorithms and graphical processing unit (GPU) computing strategies will therefore be crucial [91–93].

Acknowledgments

This work was supported by the Research Foundation Flanders (FWO, Belgium) under Grant G.0368.15N, G.0369.15N, and G.0267.18N, by personal FWO Grants to K. H. W. van den Bos, T. Altantzis, and A. De Backer, and the European Research Council under Grant 335078 COLOURATOM to S. Bals. The authors would like to thank the colleagues who have contributed to this work over the years, including A. M. Abakumov, K. J. Batenburg, E. Countiño-Gonzalez, C. de Mello Donega, R. Erni, J. J. Geuchies, B. Goris, J. Hofkens, L. Jones, P. Lievens, L. M. Liz-Marzán, I. Lobato, G. T. Martinez, P. D. Nellist, B. Partoens, M. B. J. Roeffaers, M.D. Rossell, B. Schoeters, M. J. Van Bael, W. van der Stam, M. van Huis, G. Van Tendeloo, D. Vanmaekelbergh, and N. Winckelmans.

Disclosure statement

No potential conflict of interest was reported by the authors.

Funding

This work was supported by the FP7 Ideas: European Research Council 335078 COLOURATOM;Fonds Wetenschappelijk Onderzoek G.0267.18N,G.0368.15N,G.0369.15N

ORCID

Karel Hendrik Wouter van den Bos http://orcid.org/0000-0001-7353-735X
Thomas Altantzis http://orcid.org/0000-0002-4940-7931
Sandra Van Aert http://orcid.org/0000-0001-9603-8764
Sara Bals http://orcid.org/0000-0002-4249-8017

References

[1] E. Roduner, Chem. Soc. Rev 35 (2006) p. 583. doi:10.1039/b502142c.
[2] T. Huang and X.-H.N. Xu, J. Mater. Chem 20 (2010) p. 9867. doi:10.1039/c0jm01990a.
[3] G.B. Olson, Science 277 (1997) p. 1237. doi:10.1126/science.277.5330.1237.

[4] G.B. Olson, Science 288 (2000) p. 993. doi:10.1126/science.288.5468.993.
[5] M.A. Reed and J.M. Tour, Sci. Am 282 (2000) p. 86. doi:10.1038/scientificamerican0600-86.
[6] S.J. Pennycook and L.A. Boatner, Nature 336 (1988) p. 565. doi:10.1038/336780a0.
[7] P.D. Nellist and S.J. Pennycook, Ultramicroscopy 78 (1999) p. 111. doi:10.1016/S0304-3991(99)00017-0.
[8] P.E. Batson, N. Dellby and O.L. Krivanek, Nature 418 (2002) p. 617. doi:10.1038/nature00972.
[9] E. Okunishi, I. Ishikawa, H. Sawada, F. Hosokawa, M. Hori and Y. Kondo, Microsc. Microanal 15 (2009) p. 164. doi:10.1017/S1431927609093891.
[10] R. Henderson, Q. Rev. Biophys 28 (1995) p. 171. doi:10.1017/S003358350000305X.
[11] J.C.H. Spence, Mater. Sci. Eng R26 (1999) p. 1. doi:10.1016/S0927-796X(99)00005-4.
[12] J.M. Cowley, M.S. Hansen and S.-Y. Wang, Ultramicroscopy 58 (1995) p. 18. doi:10.1016/0304-3991(94)00174-L.
[13] R. Hovden and D.A. Muller, Ultramicroscopy 123 (2012) p. 59. doi:10.1016/j.ultramic.2012.04.014.
[14] P. Hartel, H. Rose and C. Dinges, Ultramicroscopy 63 (1996) p. 93. doi:10.1016/0304-3991(96)00020-4.
[15] S.J. Pennycook and P.D. Nellist (ed.), *Scanning Transmission Electron Microscopy*, Springer, New York, 2011.
[16] M. Haider, H. Rose, S. Uhlemann, E. Schwan, B. Kabius and K. Urban, Ultramicroscopy 75 (1998) p. 53. doi:10.1016/S0304-3991(98)00048-5.
[17] B. Kabius, M. Haider, S. Uhlemann, E. Schwan, K. Urban and H. Rose, J. Electron Microsc 51 (2002) p. S51. doi:10.1093/jmicro/51.Supplement.S51.
[18] R. Erni, M.D. Rossell, C. Kisielowski and U. Dahmen, Phys. Rev. Lett 102 (2009) p. 096101. doi:10.1103/PhysRevLett.102.096101.
[19] L. Jones and P.D. Nellist, Microsc. Microanal 19 (2013) p. 1050. doi:10.1017/S1431927613001402.
[20] A.B. Yankovich, B. Berkels, W. Dahmen, P. Binev, S.I. Sanchez, S.A. Bradley, A. Li, I. Szlufarska and P.M. Voyles, Nat. Commun 5 (2014) p. 4155. doi:10.1038/ncomms5972.
[21] X. Sang and J.M. LeBeau, Ultramicroscopy 138 (2014) p. 28. doi:10.1016/j.ultramic.2013.12.004.
[22] L. Jones, H. Yang, T.J. Pennycook, M.S.J. Marshall, S. Van Aert, N.D. Browning, M.R. Castell and P.D. Nellist, Adv. Struct. Chem. Imaging 1 (2015) p. 8. doi:10.1186/s40679-015-0008-4.
[23] C. Ophus, J. Ciston and C.T. Nelson, Ultramicroscopy 162 (2016) p. 1. doi:10.1016/j.ultramic.2015.12.002.
[24] S. Van Aert, J. Verbeeck, R. Erni, S. Bals, M. Luysberg, D. Van Dyck and G. Van Tendeloo, Ultramicroscopy 109 (2009) p. 1236. doi:10.1016/j.ultramic.2009.05.010.
[25] A. De Backer, K.H.W. van den Bos, W. Van den Broek, J. Sijbers and S. Van Aert, Ultramicroscopy 171 (2016) p. 104. doi:10.1016/j.ultramic.2016.08.018.
[26] K.H.W. van den Bos, F.F. Krause, A. Beché, J. Verbeeck, A. Rosenauer and S. Van Aert, Ultramicroscopy 172 (2017) p. 75. doi:10.1016/j.ultramic.2016.10.003.
[27] P.A. Midgley and M. Weyland, Ultramicroscopy 96 (2003) p. 413. doi:10.1016/S0304-3991(03)00105-0.
[28] P.A. Midgley and R.E. Dunin-Borkowski, Nat. Mater 8 (2009) p. 271. doi:10.1038/nmat2406.
[29] M. Ohwada, K. Kimoto, T. Mizoguchi, Y. Ebina and T. Sasaki, Sci. Rep 3 (2013) p. 2801. doi:10.1038/srep02801.

[30] T. Altantzis, E. Countiño-Gonzalez, W. Baekelant, G.T. Martinez, A.M. Abakumov, G. Van Tendeloo, M.B.J. Roeffaers, S. Bals and J. Hofkens, ACS Nano 10 (2016) p. 7604. doi:10.1021/acsnano.6b02834.
[31] G. De Cremer, E. Countiño-Gonzalez, M.B.J. Roefaers, B. Moens, J. Ollevier, M. Van der Auweraer, R. Schoonheydt, P.A. Jacobs, F.C. De Schryver, J. Hofkens, D.E. De Vos, B.F. Sels and T. Vosch, J. Am. Chem. Soc 131 (2009) p. 3049. doi:10.1021/ja810071s.
[32] Y. Sasaki and T. Suzuki, Mater. Trans 50 (2009) p. 1050. doi:10.2320/matertrans.MC200809.
[33] A. Mayoral, T. Carey, P.A. Anderson, A. Lubk and I. Diaz, Angew. Chem., Int. Ed. 50 (2011) p. 11230. doi:10.1002/anie.201105450.
[34] A. Mayoral, T. Carey, P.A. Anderson and I. Diaz, Microporous Mesoporous Mater 166 (2013) p. 117. doi:10.1016/j.micromeso.2012.04.033.
[35] A.J. den Dekker, S. Van Aert, A. van den Bos and D. Van Dyck, Ultramicroscopy 104 (2005) p. 83. doi:10.1016/j.ultramic.2005.03.001.
[36] S. Van Aert, A.J. den Dekker, A. van den Bos, D. Van Dyck and J.H. Chen, Ultramicroscopy 104 (2005) p. 107. doi:10.1016/j.ultramic.2005.03.002.
[37] M. Huijben, G. Rijnders, D.H.A. Blank, S. Bals, S. Van Aert, J. Verbeeck, G. Van Tendeloo, A. Brinkman and H. Hilgenkamp, Nat. Mater 5 (2006) p. 556. doi:10.1038/nmat1675.
[38] S. Van Aert, S. Turner, R. Delville, D. Schryvers and G. Van Tendeloo, Adv. Mater 24 (2012) p. 523. doi:10.1002/adma.201103717.
[39] D. Van Dyck, Adv.Imag. Elect. Phys 123 (2002) p. 105.
[40] P.D. Nellist, *Scanning transmission electron microscopy*, in *Science of Microscopy*, P. Hawkes and J.C.H. Spence, eds., Springer, New York, 2007, p. 65.
[41] W. van der Stam, J.J. Geuchies, T. Altantzis, K.H.W. van den Bos, J.D. Meeldijk, S. Van Aert, S. Bals, D. Vanmaekelbergh and C. De Mello Donega, J. Am. Chem. Soc 139 (2017) p. 4087. doi:10.1021/jacs.6b13079.
[42] P. Cottingham and R.L. Brutchey, Chem. Commun 52 (2016) p. 5246. doi:10.1039/C6CC01088A.
[43] P.W. Atkins, T. Overton, J. Rourke, M. Weller and F. Armstrong, *Shriver & Atkins' Inorganic Chemistry*, Oxford University Press, Oxford, 2010.
[44] S. Bals, S. Van Aert and G. Van Tendeloo, Curr. Opin. Solid State Mater. Sci. 17 (2013) p. 107. doi:10.1016/j.cossms.2013.03.001.
[45] L. Houben and M.B. Sadan, Ultramicroscopy 111 (2011) p. 1512. doi:10.1016/j.ultramic.2011.06.001.
[46] M.C. Scott, -C.-C. Chen, M. Mecklenburg, C. Zhu, R. Xu, P. Ercius, U. Dahmen, B. C. Regan and J. Miao, Nature 483 (2012) p. 444. doi:10.1038/nature10843.
[47] N. Goubet, C. Yan, D. Polli, H. Portales, I. Arfaoui, G. Cerullo and M.P. Pileni, Nano Lett 13 (2013) p. 504. doi:10.1021/nl303898y.
[48] C. Louis and O. Pluchery, *Gold Nanoparticles for Physics, Chemistry and Biology*, Imperial College Press, London, 2012.
[49] Z.Y. Li, N.P. Young, M. Di Vece, S. Palomba, R.E. Palmer, A.L. Bleloch, B.C. Curley, R. L. Johnston, J. Jiang and J. Yuan, Nature 451 (2008) p. 46. doi:10.1038/nature06470.
[50] S. Van Aert, K.J. Batenburg, M.D. Rossell, R. Erni and G. Van Tendeloo, Nature 470 (2011) p. 374. doi:10.1038/nature09771.
[51] H.E, K.E. MacArthur, T.J. Pennycook, E. Okunishi, A.J. D'Alfonso, N.R. Lugg, L.J. Allen and P.D. Nellist, Ultramicroscopy 133 (2013) p. 109. doi:10.1016/j.ultramic.2013.07.002.
[52] S. Van Aert, A. De Backer, G.T. Martinez, B. Goris, S. Bals and G. Van Tendeloo, Phys. Rev. B 87 (2013) p. 064107. doi:10.1103/PhysRevB.87.064107.

[53] A. De Backer, G.T. Martinez, A. Rosenauer and S. Van Aert, Ultramicroscopy 134 (2013) p. 23. doi:10.1016/j.ultramic.2013.05.003.
[54] G.T. Martinez, A. De Backer, A. Rosenauer, J. Verbeeck and S. Van Aert, Micron 63 (2014) p. 57. doi:10.1016/j.micron.2013.12.009.
[55] K.E. MacArthur, A.J. D'Alfonso, D. Ozkaya, L.J. Allen and P.D. Nellist, Ultramicroscopy 156 (2015) p. 1. doi:10.1016/j.ultramic.2015.04.010.
[56] G.T. Martinez, A. Rosenauer, A. De Backer, J. Verbeeck and S. Van Aert, Ultramicroscopy 137 (2014) p. 12. doi:10.1016/j.ultramic.2013.11.001.
[57] S. Bals, M. Casavola, M.A. van Huis, S. Van Aert, K.J. Batenburg, G. Van Tendeloo and D. Vanmaekelbergh, Nano Lett 11 (2011) p. 3420. doi:10.1021/nl201212n.
[58] B. Goris, S. Bals, W. Van den Broek, E. Carbó-Argibay, S. Gómez-Graña, L.M. Liz-Marzán and G. Van Tendeloo, Nat. Mater 11 (2012) p. 930. doi:10.1038/nmat3462.
[59] B. Goris, A. De Backer, S. Van Aert, S. Gómez-Graña, L.M. Liz-Marzán, G. Van Tendeloo and S. Bals, Nano Lett 13 (2013) p. 4236. doi:10.1021/nl401945b.
[60] M. Bar Sadan, L. Houben, S.G. Wolf, A. Enyashin, G. Seifert, R. Tenne and K. Urban, Nano Lett 8 (2008) p. 891. doi:10.1021/nl073149i.
[61] C.-C. Chen, C. Zhu, E.R. White, C.-Y. Chiu, M.C. Scott, B.C. Regan, L.D. Marks, Y. Huang and J. Miao, Nature 496 (2013) p. 74. doi:10.1038/nature12050.
[62] B. Goris, J. De Beenhouwer, A. De Backer, D. Zanaga, K.J. Batenburg, A. Sánchez-Iglesias, L.M. Liz-Marzán, S. Van Aert, S. Bals, J. Sijbers and G. Van Tendeloo, Nano Lett 15 (2015) p. 6996. doi:10.1021/nl504066f.
[63] Y. Yang, -C.-C. Chen, M.C. Scott, C. Ophus, R. Xu, A. Pryor, L. Wu, F. Sun, W. Theis, J. Zhou, M. Eisenbach, P.R.C. Kent, R.F. Sabirianov, H. Zeng, P. Ercius and J. Miao, Nature 542 (2017) p. 75. doi:10.1038/nature21048.
[64] T. Willhammar, K. Sentosun, S. Mourdikoudis, B. Goris, M. Kurttepeli, M. Bercx, D. Lamoen, B. Partoens, I. Pastoriza-Santos, J. Pérez-Juste, L.M. Liz-Marzán, S. Bals and G. Van Tendeloo, Nat. Commun 8 (2017) p. 14925. doi:10.1038/ncomms14925.
[65] K. Tedsree, T. Li, S. Jones, C.W.A. Chan, K.M.K. Yu, P.A.J. Bagot, E.A. Marquis, G.D.W. Smith and S.C.E. Tsang, Nat. Nanotechnol 6 (2011) p. 302. doi:10.1038/nnano.2011.42.
[66] R. Huang, Y.-H. Wen, Z.Z. Zhu and S.-G. Sun, J. Phys. Chem. C 116 (2012) p. 8664. doi:10.1021/jp3015639.
[67] H. Akamine, K.H.W. van den Bos, N. Gauquelin, S. Farjami, S. Van Aert, D. Schryvers and M. Nishida, J. Alloys Compd 644 (2015) p. 570. doi:10.1016/j.jallcom.2015.04.205.
[68] K.H.W. van den Bos, A. De Backer, G.T. Martinez, N. Winckelmans, S. Bals, P.D. Nellist and S. Van Aert, Phys. Rev. Lett 116 (2016) p. 246101. doi:10.1103/PhysRevLett.116.246101.
[69] L. Jones, K.E. MacArthur, V.T. Fauske, A.T.J. van Helvoort and P.D. Nellist, Nano Lett 14 (2014) p. 6336. doi:10.1021/nl501233g.
[70] J.J. Geuchies, C. Van Overbeek, W.H. Evers, B. Goris, A. De Backer, A.P. Gantapara, F.T. Rabouw, J. Hilhorst, J.L. Peters, O. Konovalov, A.V. Petukhov, M. Dijkstra, L.D.A. Siebbeles, S. Van Aert, S. Bals and D. Vanmaekelbergh, Nat. Mater 15 (2016) p. 1248. doi:10.1038/nmat4746.
[71] E. Kalesaki, W.H. Evers, G. Allan, D. Vanmaekelbergh and C. Delerue, Phys. Rev. B 88 (2013) p. 115431. doi:10.1103/PhysRevB.88.115431.
[72] W.H. Evers, J.M. Schins, M. Aerts, A. Kulkarni, P. Capiod, M. Berthe, B. Grandidier, C. Delerue, H.S.J. van der Zant, C. van Overbeek, J.L. Peters, D. Vanmaekelbergh and L.D.D. Siebbeles, Nat. Commun 6 (2015) p. 8195. doi:10.1038/ncomms9195.
[73] J.L. Peters, K.H.W. van den Bos, S. Van Aert, B. Goris, S. Bals and D. Vanmaekelbergh, Chem. Mater 29 (2017) p. 4122. doi:10.1021/acs.chemmater.7b01103.

[74] A. De Backer, L. Jones, T. Altantzis, B. Goris, P.D. Nellist, S. Bals and S. Van Aert, Nanoscale 9 (2017) p. 8791. doi:10.1039/C7NR02656K.
[75] S. Bals, S. Van Aert, C.P. Romero, K. Lauwaet, M.J. Van Bael, B. Schoeters, B. Partoens, E. Yücelen, P. Lievens and G. Van Tendeloo, Nat. Commun 3 (2012) p. 897. doi:10.1038/ncomms1887.
[76] A.J. den Dekker, J. Sijbers and D. Van Dyck, J. Microsc 194 (1999) p. 95. doi:10.1111/jmi.1999.194.1.95.
[77] S. Van Aert, A.J. den Dekker, D. Van Dyck and A. Van Den Bos, Ultramicroscopy 90 (2002) p. 273. doi:10.1016/S0304-3991(01)00152-8.
[78] S. Van Aert, A.J. den Dekker, A. van den Bos and D. Van Dyck, Adv. Imag. Elect. Phys 130 (2004) p. 1.
[79] A.J. den Dekker, J. Gonnissen, A. De Backer, J. Sijbers and S. Van Aert, Ultramicroscopy 134 (2013) p. 34. doi:10.1016/j.ultramic.2013.05.017.
[80] J. Gonnissen, A. De Backer, A.J. den Dekker, G.T. Martinez, A. Rosenauer, J. Sijbers and S. Van Aert, Appl. Phys. Lett 105 (2014) p. 063116. doi:10.1063/1.4892884.
[81] A. De Backer, A. De wael, J. Gonnissen and S. Van Aert, Ultramicroscopy 151 (2015) p. 46. doi:10.1016/j.ultramic.2014.10.015.
[82] N. Shibata, Y. Kohno, S.D. Findlay, H. Sawada, Y. Kondo and Y. Ikuhara, J. Electron Microsc 59 (2010) p. 473. doi:10.1093/jmicro/dfq014.
[83] K. Müller-Caspary, O. Oppermann, T. Grieb, F.F. Krause, A. Rosenauer, M. Schowalter, T. Mehrtens, A. Beyer, K. Volz and P. Potapov, Sci. Rep 6 (2016) p. 37146. doi:10.1038/srep37146.
[84] J.Y. Zhang, J. Hwang, B.J. Isaac and S. Stemmer, Sci. Rep 5 (2015) p. 12419. doi:10.1038/srep12419.
[85] K. Sentosun, M.N. Sanz Ortiz, K.J. Batenburg, L.M. Liz-Marzán and S. Bals, Part. Part. Syst. Charact 32 (2015) p. 1063. doi:10.1002/ppsc.201500097.
[86] T.J. Pennycook, A.R. Lupini, H. Yang, M.F. Murfitt, L. Jones and P.D. Nellist, Ultramicroscopy 151 (2015) p. 160. doi:10.1016/j.ultramic.2014.09.013.
[87] H. Yang, T.J. Pennycook and P.D. Nellist, Ultramicroscopy 151 (2015) p. 232. doi:10.1016/j.ultramic.2014.10.013.
[88] K. Müller, H. Ryll, I. Ordavo, S. Ihle, L. Strüder, K. Volz, J. Zweck, H. Soltau and A. Rosenauer, Appl. Phys. Lett 101 (2012) p. 212110. doi:10.1063/1.4767655.
[89] V.B. Ozdol, C. Gammer, X.G. Jin, P. Ercius, C. Ophus, J. Ciston and A.M. Minor, Appl. Phys. Lett 106 (2015) p. 253107. doi:10.1063/1.4922994.
[90] M.W. Tate, P. Purohit, D. Chamberlain, K.X. Nguyen, R. Hovden, C.S. Chang, P. Deb, E. Turgut, J.T. Heron, D.G. Schlom, D.C. Ralph, G.D. Fuchs, K.S. Shanks, H.T. Philipp, D.A. Muller and S.M. Gruner, Microsc. Microanal 22 (2016) p. 237. doi:10.1017/S1431927615015664.
[91] C. Dwyer, Ultramicroscopy 110 (2010) p. 195. doi:10.1016/j.ultramic.2009.11.009.
[92] I. Lobato and D. Van Dyck, Ultramicroscopy 156 (2015) p. 9. doi:10.1016/j.ultramic.2015.04.016.
[93] M. Yu, A.B. Yankovich, A. Kaczmarowski, D. Morgan and P.M. Voyles, ACS Nano 10 (2016) p. 4031. doi:10.1021/acsnano.5b05722.